

Multifragmentation in Xe(50A MeV)+Sn

Confrontation of theory and data

Regina Nebauer^{1,2}, Jörg Aichelin¹

and the INDRA collaboration

M. Assenard¹, G. Auger³, Ch.O. Bacri⁴, F. Bocage⁵, R. Bougault⁵, R. Brou⁵, P. Buchet⁶, J.L. Charvet⁶, A. Chbihi³, J. Colin⁵, D. Cussol⁵, R. Dayras⁶, A. Demeyer⁷, D. Doré⁶, D. Durand⁵, P. Eudes¹, E. Galichet⁷, E. Genouin-Duhamel⁵, E. Gerlic⁷, M. Germain¹, D. Gourio¹, D. Guinet⁷, P. Lautyresse⁷, J.L. Laville³, T. Lefort⁵, R. Legrain⁶, N. Le Neindre⁵, O. Lopez⁵, M. Louvel⁵, A.M. Maskay⁷, L. Nalpas⁶,c A.D. Nguyen⁵, M. Parlog⁸, J. Péter⁵, A. Rahmani¹, T. Reposeur¹, E. Rosato⁹, F. Saint-Laurent³, S. Salou³, J.C. Steckmeyer⁵, M. Stern⁷, G. Tabacaru⁸, B. Tamain⁵, L. Tassan-Got⁴, O. Tirel³, E. Vient⁵, C. Volant⁶, J.P. Wieleczko³

¹ *SUBATECH, IN2P3-CNRS et Université, F-44072 Nantes Cedex 03, France.*

² *Institute for Theoretical Physics Universität Rostock, Rostock, Germany.*

³ *GANIL, CEA, IN2P3-CNRS, B.P. 5027, F-14021 Caen Cedex, France.*

⁴ *Institut de Physique Nucléaire, IN2P3-CNRS, 91406 Orsay Cedex, France.*

⁵ *LPC, IN2P3-CNRS, ISMRA et Université, F-14050 Caen Cedex, France.*

⁶ *DAPNIA/SPhN, CEA/Saclay, 91191 Gif sur Yvette Cedex, France.*

⁷ *IPN Lyon, IN2P3-CNRS et Université, F-69622 Villeurbanne Cedex, France.*

⁸ *Nuclear Institute for Physics and Nuclear Engineering, Bucharest, Romania.*

⁹ *Dipartimento di Scienze Fisiche, Univ. di Napoli, I-180126 Napoli, Italy.*

We compare in detail central collisions Xe(50A MeV) + Sn, recently measured by the INDRA collaboration, with the Quantum Molecular Dynamics (QMD) model in order to identify the reaction mechanism which leads to multifragmentation. We find that QMD describes the data quite well, in the projectile/target region as well as in the midrapidity zone where also statistical models can be and have been employed. The agreement between QMD and data allows to use this dynamical model to investigate the reaction in detail. We arrive at the following observations: a) the in medium nucleon nucleon cross section is not significantly different from the free cross section, b) even the most central collisions have a binary character, c) most of the fragments are produced in the

central collisions and d) the simulations as well as the data show a strong attractive in-plane flow resembling deep inelastic collisions e) at midrapidity the results from QMD and those from statistical model calculations agree for almost all observables with the exception of $\frac{d^2\sigma}{dZdE}$. This renders it difficult to extract the reaction mechanism from midrapidity fragments only. According to the simulations the reaction shows a very early formation of fragments, even in central collisions, which pass through the reaction zone without being destroyed. The final transverse momentum of the fragments is very close to the initial one and due to the Fermi motion. A heating up of the systems is not observed and hence a thermal origin of the spectra cannot be confirmed.

I. INTRODUCTION

Why does a nucleus shatter into several (up to a dozen) intermediate mass fragments (IMF's, $Z \geq 3$) if hit by a projectile nucleus? Is this only a statistical or even a thermal process and hence (micro)canonical phase space models are the proper tool for its description [1] - [6] or is this a dynamical process, for example similar to the shattering of glass, as also conjectured [7]?

Despite of extensive efforts of several experimental groups [8] - [13] this question is not finally decided yet. The main reason is that, surprisingly enough, both approaches give very similar results for at least two key observables. If multifragmentation is a thermal process and due to the liquid gas phase transition, predicted by the nuclear matter Hamiltonian for a density around a third of normal nuclear matter density, one expects a mass yield curve of the form of a power law $\sigma(A) \propto A^{-\tau}$. The same is true if multifragmentation is a process similar to the shattering of glass [7]. If multifragmentation is a slow process and the system reaches and maintains a global equilibrium before it fragments, the average transverse kinetic energy of the fragments is equals $3/2$ kT and independent of the fragments size. If the opposite is true and multifragmentation is a very fast process in which the fragments retain their initial Fermi momentum the fragments have as well a transverse kinetic energy independent of their mass of $2/5E_F$ [14], where E_F is the Fermi energy of the nucleus. Hence neither the mass yield curve nor the average kinetic energies of fragments allow for a distinction between the two quite different mechanisms. Rather one has to study more exclusive observables or many

body correlations. This requires usually high statistics 4π experiments.

There are further complications. One expects that the reaction mechanism depends on the impact parameter. To understand details of the reaction or even the reaction mechanism from inclusive data has turned out to be hopeless. Thus an effective event selection is necessary. At low beam energies ($30A \text{ MeV} < E_{kin} < 150A \text{ MeV}$) such a selection is difficult because the available phase space is very small and hence it is not easy to find effective selection criteria. The most useful event selection criteria like charged particle multiplicity or total transverse energy require high granularity 4π detectors specially devoted to study multifragmentation.

These high granularity low threshold 4π detectors became available only recently at the GSI in Darmstadt (Germany), at GANIL in Caen (France) and at the Michigan State University (USA). The results from these detectors allow now for a new effort to understand multifragmentation.

It is the purpose of this paper to compare in detail the recently obtained experimental results of the INDRA collaboration for the reaction $\text{Xe}(50A \text{ MeV}) + \text{Sn}$ with the predictions of the Quantum Molecular Dynamics (QMD) approach, a dynamical model suited to describe the formation of fragments. This reaction has been chosen for two reasons. First of all, the INDRA detector has the highest efficiency of all presently operating 4π detectors and therefore the results present a challenge for every theory. Secondly, at $50A \text{ MeV}$ the number of produced fragments has a maximum [15] and therefore it is the proper energy to study multifragmentation. It is also an energy where the Fermi spheres of projectile and target become separated and hence one may expect that it is the beginning of the transitional regime between low energy heavy ion reactions, characterized by compound nucleus formation and deep inelastic collisions, and high energy heavy ion reactions, characterized by two types of nucleons, the participants and the spectators.

We start out with a short description of the QMD model in section II. A comparison of simulations with experiment sounds easier than it is. In order to compare them it is necessary to employ a filter which tells us how the detector would register the theoretical data. It has to determine how the detector reacts if hit by 2 particles in the same reaction, whether a particle has hit the active zone of one of the detectors and whether the particle has an energy below the (detector dependent) threshold and hence is not registered. It has as well to take into account the deceleration of the particles while passing through the target. The filter is not only of importance for the prediction of single particle observables but as well for the proper selection of the subset of data which are the basis of the analysis. Thus an event selection is necessary if one wants to select a small impact parameter range. Therefore, in section III, we discuss the

influence of the filter on the theoretical QMD data and motivate our criterion for selecting the most central events. Section V presents the single particle spectra for light charged particles followed by an analysis of the global fragment observables in section VI. As we will see in section VII, we can separate two angular ranges. In the nucleus nucleus center of mass frame the angular distribution is flat between $\theta = 60^\circ$ and $\theta = 120^\circ$. For smaller or larger angles the angular distribution increases towards the beam axis. We analyze both regions separately in sections VIII and IX. Section X is devoted to a discussion of other proposed criteria to select central events and we compare the results obtained under these selection criteria with those obtained with our choice. Finally, in section XI, we discuss the reaction scenario which emerges from the simulations and draw our conclusions.

II. QMD MODEL

The QMD model is a time dependent A-body theory to simulate the time evolution of heavy ion reactions on an event by event basis. It is based on a generalized variational principle. As every variational approach it requires the choice of a test wave function ϕ . In the QMD approach this is an A-body wave function with 6 A time dependent parameters if the nuclear system contains A nucleons.

To calculate the time evolution of the system we start out from the action

$$S = \int_{t_1}^{t_2} \mathcal{L} [\phi, \phi^*] dt \quad (1)$$

with the Lagrange functional

$$\mathcal{L} = \left\langle \Phi \left| i\hbar \frac{d}{dt} - H \right| \Phi \right\rangle. \quad (2)$$

The total time derivative includes the derivation with respect to the parameters. The time evolution of the parameters is obtained by the requirement that the action is stationary under the allowed variation of the wave function. This leads to an Euler-Lagrange equation for each time dependent parameter.

The basic assumption of the QMD model is that a test wave function of the form

$$\Phi = \prod_{i=1}^{A_T+A_P} \phi_i \quad (3)$$

with

$$\phi_i(\vec{r}, t) = \left(\frac{2}{L\pi} \right)^{3/4} e^{-(\vec{r}-\vec{r}_i(t))^2/4L} e^{i(\vec{r}-\vec{r}_i(t))\vec{p}_i(t)} e^{ip_i^2(t)t/2m}. \quad (4)$$

is a good approximation to the nuclear wave function. The time dependent parameters are $\vec{r}_i(t), \vec{p}_i(t)$, L is fixed and equals 1.08 fm^2 . Thus the rms radius of a nucleon is about 1.8 fm and hence almost twice as large as that obtained from electron scattering. A smaller value of L is excluded because the nuclei would become unstable after initialization. Thus this value of L presents the limit for a semiclassical theory. The consequences of this, longer interaction range will be discussed along this article.

Variation yields:

$$\dot{\vec{r}}_i = \frac{\vec{p}_i}{m} + \nabla_{\vec{p}_i} \sum_j \langle V_{ij} \rangle = \nabla_{\vec{p}_i} \langle H \rangle \quad (5)$$

$$\dot{\vec{p}}_i = -\nabla_{\vec{r}_i} \sum_{j \neq i} \langle V_{ij} \rangle = -\nabla_{\vec{r}_i} \langle H \rangle \quad (6)$$

with $\langle V_{ij} \rangle = \int d^3x_1 d^3x_2 \phi_i^* \phi_j^* V(x_1, x_2) \phi_i \phi_j$. These are the time evolution equations which are solved numerically. Thus the variational principle reduces the time evolution of the n -body Schrödinger equation to the time evolution equations of $6 \cdot (A_P + A_T)$ parameters to which a physical meaning can be attributed.

The nuclear dynamics of the QMD can also be translated into a semiclassical scheme. The Wigner distribution function f_i of the nucleon i can be easily derived from the test wave functions (note that antisymmetrization is neglected)

$$f_i(\vec{r}, \vec{p}, t) = \frac{1}{\pi^3 \hbar^3} e^{-(\vec{r} - \vec{r}_i(t))^2 \frac{1}{2L}} e^{-(\vec{p} - \vec{p}_i(t))^2 \frac{2L}{\hbar^2}} \quad (7)$$

and the total one body Wigner density is the sum of those of all nucleons. The potential can be calculated with help of the wave function or of the Wigner density. Hence the expectation value of the total Hamiltonian reads

$$\begin{aligned} \langle H \rangle &= \langle T \rangle + \langle V \rangle \\ &= \sum_i \frac{p_i^2}{2m_i} + \sum_i \sum_{j>i} \int f_i(\vec{r}, \vec{p}, t) V^{ij} f_j(\vec{r}', \vec{p}', t) d\vec{r} d\vec{r}' d\vec{p} d\vec{p}' \quad . \end{aligned} \quad (8)$$

The baryon-baryon potential V_{ij} consists of the real part of the Brückner G -Matrix which is supplemented by an effective Coulomb interaction between the charged particles. The former can be further subdivided into a part containing the contact Skyrme-type interaction only and a contribution due to a finite range Yukawa-potential. V^{ij} consists of

$$\begin{aligned} V^{ij} &= G^{ij} + V_{\text{Coul}}^{ij} \\ &= V_{\text{Skyrme}}^{ij} + V_{\text{Yuk}}^{ij} + V_{\text{Coul}}^{ij} \\ &= t_1 \delta(\vec{x}_i - \vec{x}_j) + t_2 \delta(\vec{x}_i - \vec{x}_j) \rho^{\gamma-1}(\vec{x}_i) + t_3 \frac{\exp\{-|\vec{x}_i - \vec{x}_j|/\mu\}}{|\vec{x}_i - \vec{x}_j|/\mu} \\ &\quad + \frac{Z_i Z_j e^2}{|\vec{x}_i - \vec{x}_j|} \end{aligned} \quad (9)$$

The range of the Yukawa-potential is chosen as 1.5 fm. Z_i, Z_j are the effective charges $\frac{Z_p}{N_p}, \frac{Z_t}{N_t}$ of the baryons i and j . The real part of the Brückner G -matrix is density dependent, which is reflected in the expression for G^{ij} . The expectation value of G for the nucleon i is a function of the interaction density ρ_{int}^i .

$$\rho_{\text{int}}^i(\vec{r}_i) = \frac{1}{(\pi L)^{3/2}} \sum_{j \neq i} e^{-(\vec{r}_i - \vec{r}_j)^2 / L} \quad (10)$$

Note that the interaction density has twice the width of the single particle density.

The imaginary part of the G-matrix acts like a collision term. In the QMD simulations we restrict ourselves to binary collisions (two-body level). The collisions are performed in a point-particle sense in a similar way as in VUU or in cascade calculations: Two particles may collide if they come closer than $r = \sqrt{\sigma/\pi}$ where σ is a parametrization of the free NN - cross section. A collision does not take place if the final state phase space of the scattered particles is already occupied by particles of the same kind (Pauli blocking).

Neglecting antisymmetrization is the most drastic approximation of the model. Thus, all properties related to shell structures cannot be accounted for. The binding energy per nucleon follows the Weizsäcker mass formula. Hence, small fragments which show a large deviation from that formula cannot be reproduced quantitatively. The initial values of the parameters are chosen in that way that the nucleons give proper densities and momentum distributions of the projectile and target nuclei.

Fragments are determined in this model by a minimum spanning tree procedure. At the end of the reaction all those nucleons are part of a fragment which have a neighbor in a distance less than $r_{frag} = 3fm$. After 200 fm/c the fragment multiplicity remains stable because only bound nucleons remain together whereas the others separate in the expanding system. The result is also not sensitive to r_{frag} in a reasonable interval for r_{frag} .

For further details of the QMD- model we refer to ref. [16,17]

To compare the QMD simulations with experimental data as realistic as possible we built up a data base of about 60 000 QMD events over a large impact parameter range. We have chosen a soft equation of state.

III. THE EXPERIMENTAL FILTER

We start our comparison of the INDRA results with QMD calculations with a discussion of the filter. To filter simulations of heavy ion collisions is an absolute must if one would like to compare experiment and calculation in a quantitative way. A filter routine is a very complicated program. It has not only to take into account which particles are not registered because they hit detector frames or disappear in the beam pipe. It also has to answer the question how the detector would react if by accident two particles enter the same detector and it has to take into account how target like fragments with a very low energy pass through the solid target material, i.e. whether they arrive at all at the detectors. In addition, it has to reproduce exactly the energy thresholds of the different detectors, which is of special importance for these low energy reactions where the thresholds are not far away from the maxima of the fragment

energy distributions. A minimum of 4 charged products is required in both the filtered QMD events as well as for the INDRA data.

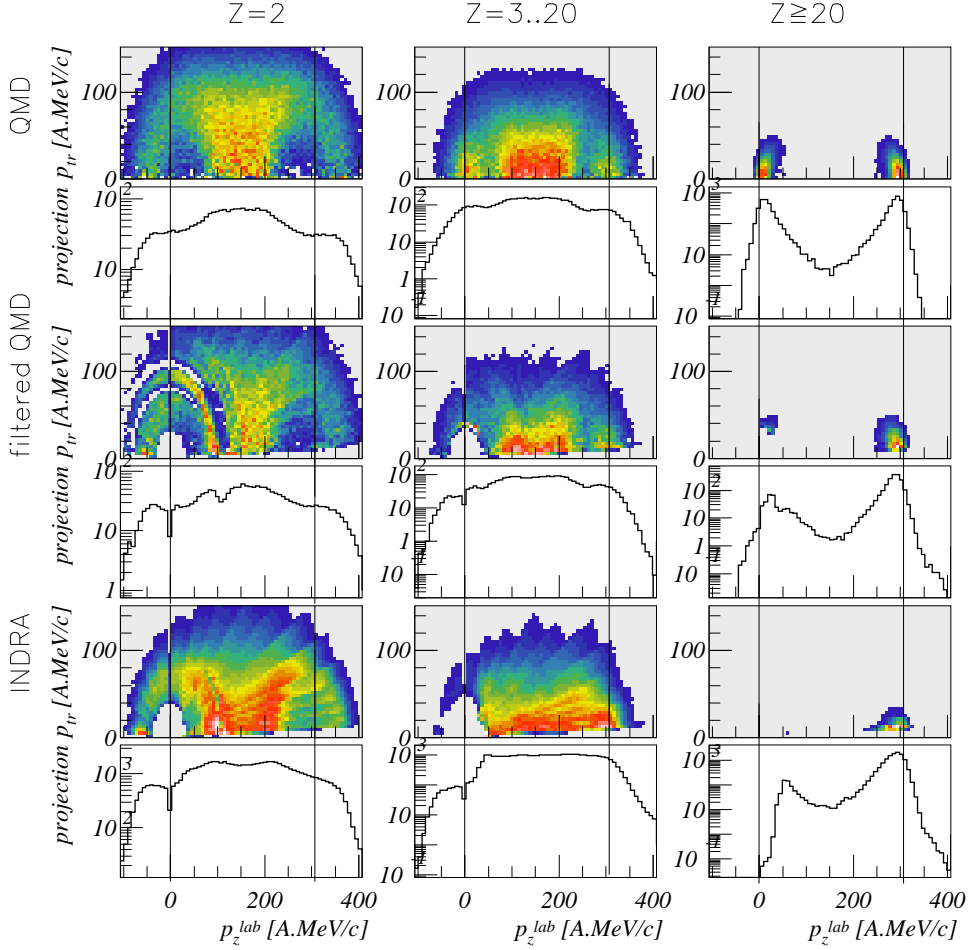


FIG. 1. *Invariant cross section plot of all events. We display QMD (top), filtered QMD (middle) and INDRA (bottom) data, the lines indicate the initial projectile and the target momenta. The color coding uses a logarithmic scale*

Fig. 1 displays the invariant cross section $\frac{d\sigma}{dp_z p_t dp_t}$ in the laboratory system for three different charge bins ($Z=2$, $3 \leq Z \leq 20$ and $Z > 20$) as well as the projection onto the p_z axis. We display this quantity for the unfiltered QMD events, for the filtered QMD events and for the INDRA data. First of all, we see the importance of the filter. It changes the distribution in a quite drastic way. We see also that the coarse features of the filtered QMD events are very similar to the INDRA data. There are, however, several discrepancies which have to be discussed in view of the event selection which is used later and in view of the comparison between theory and experiment.

The filter underestimates the blind zone of the detector around the target. This is true for

the $Z = 2$ particles but even more pronounced for the intermediate mass fragments (IMF's). We observe in addition two strong cuts of the filter for $Z = 2$ particles around $p \approx 100A \text{ MeV}/c$ and $p \approx 80A \text{ MeV}/c$ which are not present in the data on the same level.

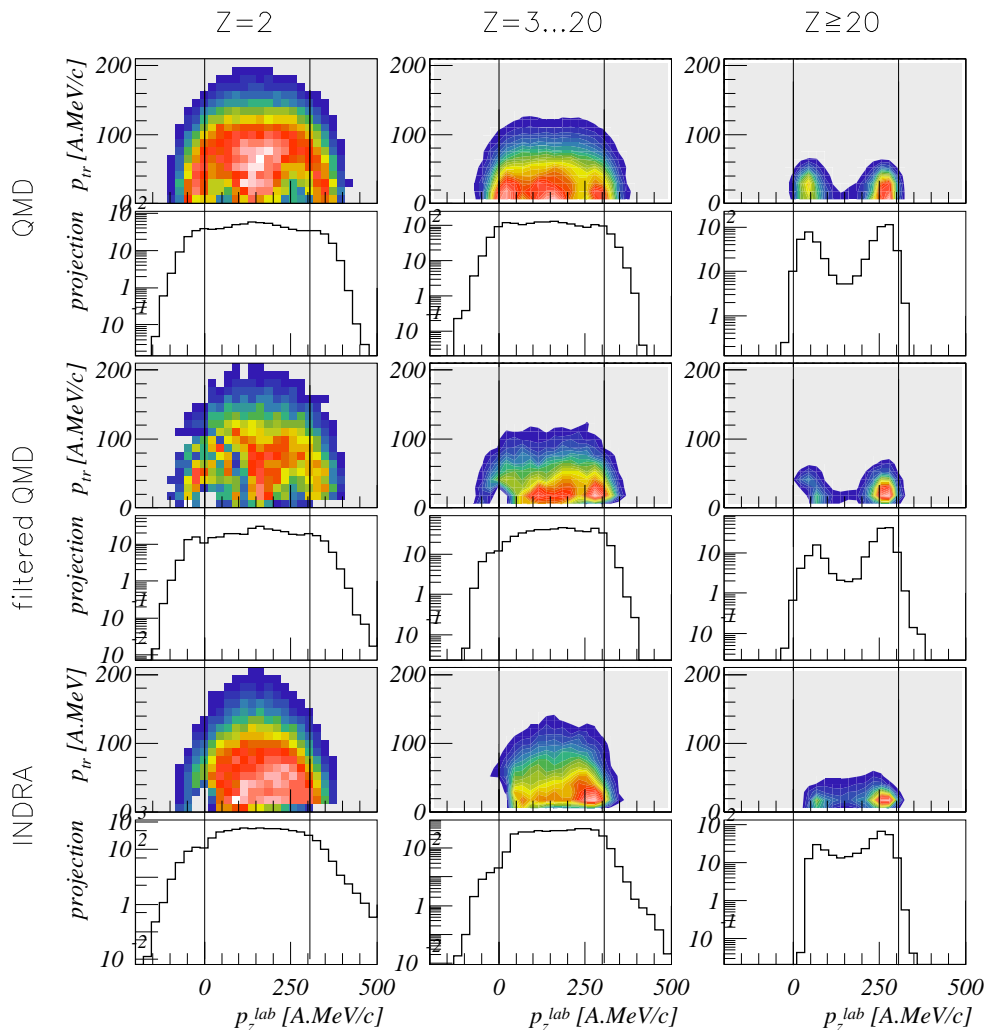


FIG. 2. Invariant cross section for central events ($E_{trans} \geq 450 \text{ MeV}$). We display QMD (top), filtered QMD (middle) and INDRA (bottom) data, the lines indicate the initial projectile and target momenta.

Whereas this observation points most probably to problems in the filter routine, the differences between filtered QMD results and INDRA data for the heavy fragments $Z \geq 20$ indicate a deficiency of the QMD program. We observe QMD events with large projectile and target remnants, in contradiction to the data. This is due to the fact that these fragments have gained a transverse in-plane momentum of about $50A \text{ MeV}/c$ which is too large as compared to the data. For the INDRA events the transverse momentum gain of these heavy remnants is slightly smaller and hence they disappear in the beam pipe. The difference is tiny as far as the energy is concerned (the additional transverse energy is less than 1 MeV) but has important conse-

quences. We expect for the QMD simulations too many events with large projectile and/or target remnants.

The overall structure of the simulated events is rather similar to that of the INDRA data and hence it is meaningful to proceed further and to select central events. As discussed in the next section this is done by the requirement that the total transverse energy of the light charged particles is larger than 450 MeV. Before we discuss the reason for this choice it is useful to investigate the influence of the filter on this small subset of events (cross section $\approx 300mb$)

Therefore, in fig. 2 we display the same quantities as in fig. 1 but for central events only. We see that also for central events the above mentioned discrepancies between filtered simulations and INDRA data persist. In the target region too many heavy fragments are observed as compared to the data, nevertheless the global event structure is again very similar.

IV. EVENT SELECTION AND IMPACT PARAMETER ESTIMATION

It is the purpose of this article to study central collisions of the system Xe(50A MeV)+Sn which has recently been measured by the INDRA collaboration. The central collisions are the most interesting ones because they yield the largest number of fragments and they are those for which the system may come to thermal equilibrium.

How can central collisions be identified? An important property of the INDRA detector is its high efficiency for light charged ($Z=1,2$) particles (LCP) independent of the type of the reaction mechanism. As observed in ref. [18] the total transverse kinetic energy of the light charged particles (LCP's) serves as an indicator for the centrality of the reaction. We hence consider the transverse energy of all light charged particles

$$E_{trans} = \sum_{Z=1,2} E_i \sin^2 \Theta_i \quad (11)$$

as a measure of the impact parameter in QMD events as well as in experiment.

The comparison of theory with experiment has to be done in two steps. First we have to make sure that QMD reproduces the measured transverse energy distribution of light charged particles. If this is the case, the same cut in E_{trans} selects the same centrality in theory and in experiment. In figure 3, left hand side, we present the transverse energy spectra for QMD simulations and for the INDRA data. We find that the QMD model reproduces the cross section $\frac{d^2\sigma}{dE_{trans}}$ quite reasonably, (thus the single particle dynamics is well described in QMD) and can be used to characterize the events. For small transverse energies the deviation is due to the limitation of the calculations to $b \leq 12$. This observation allows already to draw the first

conclusion. It points to the fact that the in medium nucleon nucleon cross section is not very different from its free counterpart. Even a mild change on the 20% level of the cross section would have given rise to a quite different stopping and hence to a quite different transverse energy of the LCP's.

One should, however, add a word of warning. QMD deals with effective charges and there is no unique prescription how to transform clusters consisting of nucleons with an effective charge to real fragments. Here we have identified a cluster containing A effective charge nucleons with the most stable nucleus of a given mass A . This procedure may violate charge conservation. A prescription which conserves strictly the total charge [19] yields a slightly different charge distribution of fragments and consequently a small change of the total transverse energy of light charged particles.

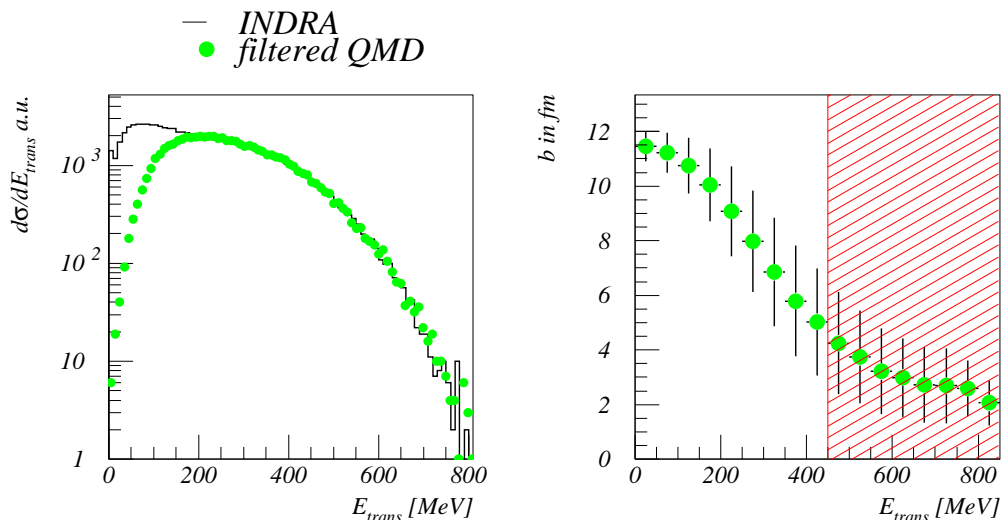


FIG. 3. *Transverse energy spectra for INDRA and filtered QMD events (left) and the correlation between the transverse energy and the impact parameter for filtered QMD calculations (right). The error bars represent the standard deviation. The spectra are normalized on the maximum of the QMD spectrum.*

In figure 3, right hand side, the correlation between the impact parameter and the transverse energy, as observed in QMD, is displayed. As can be seen, the total transverse energy of the light particles permits a classification of the events according to their centrality up to an energy of about 600 MeV.

Being interested in central collisions, we will use events with $E_{trans} \geq 450$ MeV. In our simulations the average impact parameter for this choice is 3.6 fm.

Can this impact parameter dependence of the transverse energy be verified by experimental data? For this purpose we plot in fig. 4 the IMF multiplicity as observed in QMD as a function

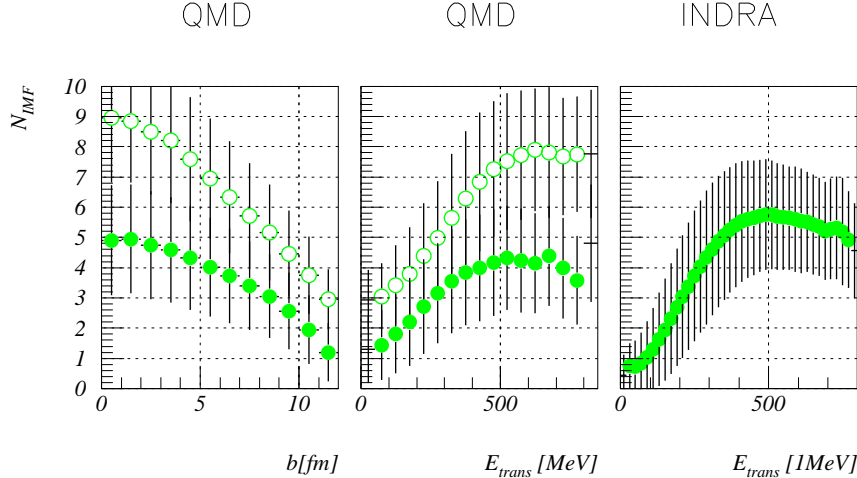


FIG. 4. Number of intermediate mass fragments observed as a function of the impact parameter (lhs) and of the total transverse energy of light particles (middle). The open circles represent the QMD simulations before being filtered, the solid circles the filtered QMD data. On the right hand side we plot the corresponding experimental results. The vertical bars mark the rms deviation.

of the impact parameter. We observe an increase of the multiplicity with increasing centrality. Despite of the large acceptance of the INDRA detector we loose about 40% of the fragments by applying the filter, mostly due to the small energy of midrapidity fragments in QMD (section VIII C).

The form of the spectra, which is very similar for QMD and INDRA data, is not changed by the filter, a reassuring fact for our event selection.

The monotonic dependence of the transverse energy and the fragment multiplicity on the impact parameter allows to eliminate the impact parameter in displaying the IMF multiplicity as a function of the transverse energy. It is displayed in the middle and the right hand side of fig. 4. We see a very good agreement of the form between theory and experiment. The absolute value of the fragment multiplicity in the simulation is about 30% too low, a consequence of the too many accepted events with large projectile/target remnants.

There exist other criteria to select the central events. It has been proposed [20,21] to use the event shape as a selection criteria and the experimental data have been analyzed using this criterion. We will discuss this alternative proposition in chapter X.

V. SINGLE PARTICLE SPECTRA

We saw in fig. 3 that the QMD calculations reproduce the total transverse kinetic energy of the light particles quite well. Now we will concentrate on central collisions and discuss whether

this good agreement holds also for the spectra of light particles. In figure 5 we plot the kinetic energy spectra for different light charged particles. In the QMD model the number of these light particles is not very well reproduced. If one analyzes the binding energy of the clusters for the Hamiltonian described in section II we find a binding energy which follows the Weizsäcker mass formula. The experimental binding energy of light clusters deviates considerably from the value predicted by this formula. Hence loosely bound clusters like ${}^3\text{He}$ are overpredicted whereas strongly bound clusters like ${}^4\text{He}$ are underpredicted. Therefore it is useless to compare the absolute number of these light fragments. However, it makes sense to compare the slope of their kinetic energy spectra which carries information about the phase space distribution of the nucleons at the point of their formation. This information should be rather independent of the observation that in QMD simulations too many (too few) of the light fragments are destroyed if their binding energy in QMD is too low (too large) as compared to the real binding energy. The slope of the light charged particles is quite well reproduced. Deviations are observed for protons and to a lesser extend for deuterons at high kinetic energy.

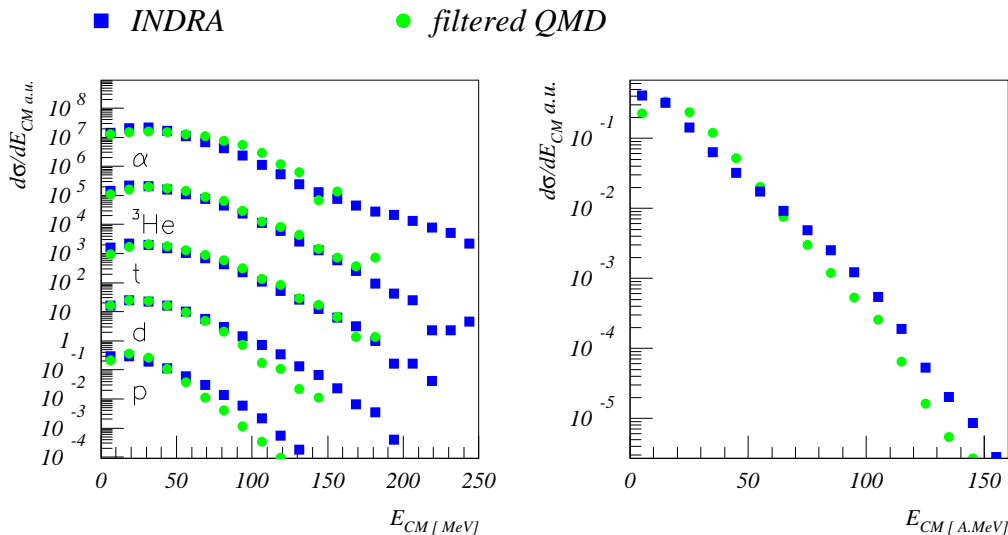


FIG. 5. Angle integrated energy spectra of light charged particles (lhs) and "protonlike" particles (rhs) for central collisions ($E_{trans} \geq 450$ MeV). The spectra are normalized on the surface

One can eliminate the problem with the absolute number of light charged particles by introducing a spectra for "protonlike" particles by giving each proton, bound in a fragment of mass A ($A < 4$), the energy E_{frag}/A . The spectra of "protonlike" particles are displayed on the right hand side of fig. 5. The mean kinetic energy /slope of the "protonlike" spectra is 20 MeV /10.5 MeV for the filtered QMD simulations and 16 MeV /12.2 MeV for the INDRA data.

VI. CHARGE-VELOCITY CORRELATIONS, CHARGE AND MULTIPLICITY DISTRIBUTIONS OF IMF'S

As already indicated in figs. 1 and 2 we observe a binary event structure in the INDRA data as well as in QMD simulations even for the most central collisions. This fact becomes even more pronounced if one displays (in fig. 6) $\frac{d\sigma}{dZ_{max}dv_z}$. For fragment emission from a statistically emitting source at rest in the center of mass one would expect the maximum of the distribution at midrapidity, clearly in contradistinction to experiment.

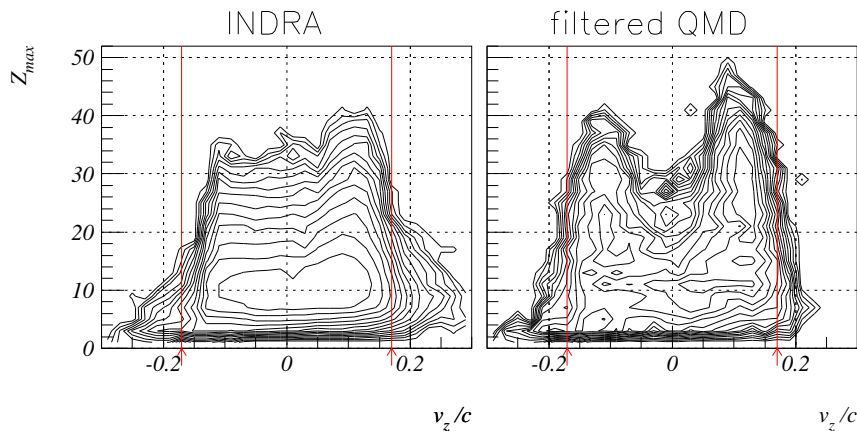


FIG. 6. *Central Collisions ($E_{trans} \geq 450$ MeV). Charge of the two biggest fragments observed as a function of the parallel velocity in the center of mass frame.*

The biggest fragments have lost about 35% of their initial velocity (marked by a line) in the data as well as in the simulations. This is remarkable: in central collisions at lower energies as well as in central collisions at higher energies we observe almost globally thermalized (sub)systems. At low energies the effective potential interaction among the nucleons, given by the real part of the Brueckner G-Matrix, is sufficiently strong to decelerate projectile and target in order to equilibrate and to form a compound nucleus. At higher energies the collisions thermalize the participants and we find in central collisions a fireball. Here, at intermediate energies, neither the effective interaction is sufficiently strong to stop projectile and target nor are the collisions sufficiently frequent because most of them are Pauli suppressed. As a consequence, we observe in this energy domain a minimum of the stopping power of nuclear matter. The present experiment confirms for the first time this theoretical prediction. The enhancement of QMD events close to projectile and target velocity, amplified by the logarithmic representation, is another time a consequence of the enhanced in-plane transverse momentum in QMD.

The charge distributions, the total multiplicity of "protonlike" particles and the IMF multiplicity for the INDRA data and the QMD simulations (central collisions, $E_{trans} \geq 450$ MeV) are shown in figure 7.

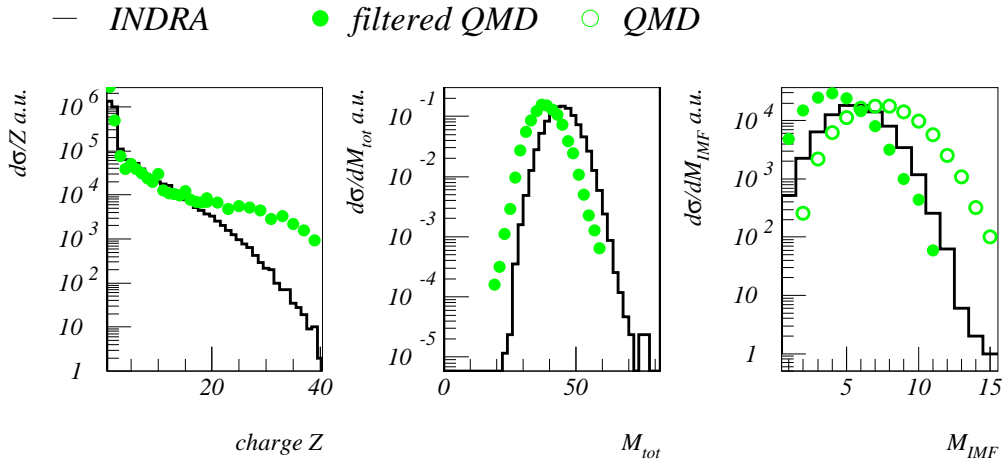


FIG. 7. Central Collisions ($E_{trans} \geq 450$ MeV). Charge distribution, total "protonlike" and IMF multiplicity distributions for INDRA data and filtered QMD calculations.

We find that QMD reproduces well the charge distribution of the fragments up to $Z \approx 15$ but overestimates the production of big fragments as already discussed. This influences the total multiplicity because events with large fragments have a lower multiplicity. The IMF multiplicity distribution (figure 7, right) gives an average value of 6.6 IMF's observed by INDRA, 5.3 IMF's for filtered QMD and 7.5 IMF's for unfiltered QMD. The fraction of events with a low IMF multiplicity is overestimated in QMD which is again a consequence of the too many events with large fragments which we observe in QMD for this event selection.

VII. ANGULAR DISTRIBUTIONS

We come now to the kinematical variables. These, as mentioned in the introduction, are the key observables for the question whether the system or a subsystem comes close to a statistical equilibrium. Statistical models have been very successfully applied to multifragmentation reactions to describe multiplicity distributions, fragment correlations and charge distributions and hence quantities related to the chemical potential [1,22]. The dynamical variables, like the kinetic energy spectra or the angular distributions, available up to now, had not been measured over a sufficient wide energy range in order to allow for a detailed comparison. With the present data this situation has changed. Hence we can address the question whether the dynamical observables show statistical features.

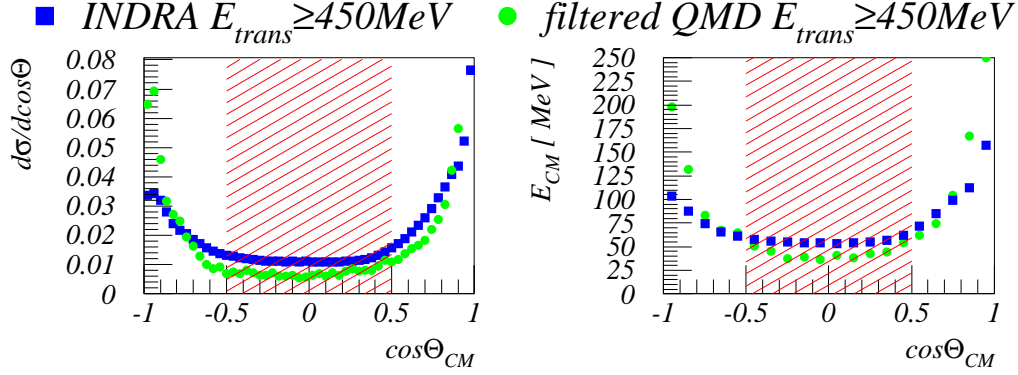


FIG. 8. Central Collisions ($E_{trans} \geq 450$ MeV). Angular distribution for IMF's and kinetic energy of the IMF's as a function of $\cos\theta$.

The angular distribution of IMF's is presented in fig. 8. We observe a flat distribution for $60^\circ \leq \theta_{CM} \leq 120^\circ$ and a strong increase of the yield in forward and backward direction for both, filtered QMD events and experiment. Also the average kinetic energy is almost constant for $60^\circ \leq \theta_{CM} \leq 120^\circ$ and shows as well an increase for angles approaching the beam axis. There the binary character of the reaction gains influence even for the central collisions.

This observation has triggered the conjecture that in these reactions indeed an equilibrated subsystem is produced which reveals itself in the midrapidity region $60^\circ \leq \theta_{CM} \leq 120^\circ$. In forward ($\theta_{CM} < 60^\circ$) and in backward ($\theta_{CM} > 120^\circ$) direction it is superimposed by preequilibrium emission. The quite different behavior makes it meaningful to separate the analysis for the two zones:

- the **midrapidity zone** which corresponds to fragments emitted in $60^\circ \leq \theta_{CM} \leq 120^\circ$,
- the **forward/backward zone** which corresponds to fragments emitted in $\theta_{CM} < 60^\circ, \theta_{CM} > 120^\circ$

VIII. EMISSION AT MIDRAPIDITY

A. Charge and IMF multiplicity distributions

The charge yield and the IMF multiplicity distribution of fragments emitted in the midrapidity zone are plotted in fig. 9. We find a good agreement between the INDRA results and QMD data. The multiplicity distribution on the right hand side is once again spoiled by the large fragment events. In this plot the distributions are normalized on the area.

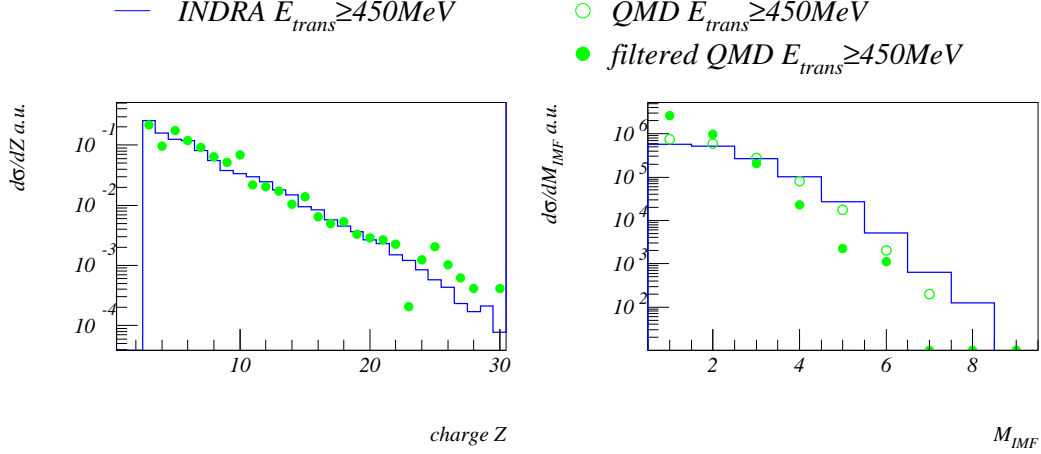


FIG. 9. Central Collisions ($E_{trans} \geq 450 MeV$). Charge ($Z \geq 3$) and IMF multiplicity distribution for the emission at $60^\circ \leq \theta_{CM} \leq 120^\circ$ for INDRA data and QMD calculations.

If we employ a rather different event selection criterion, $\theta_{flow} \geq 60^\circ$, discussed in section X, we observe almost the same charge yield as can be seen in fig. 10. In ref. [21] the charge distribution for $\theta_{flow} \geq 60^\circ$ has been compared with the prediction of a statistical model calculation using the SMM program [1,22]. The good agreement can be seen as well in fig. 10. Note that the source sizes varies, for INDRA ($\theta_{flow} \geq 60^\circ$) as well as SMM which both correspond to a single source, the source is about a factor of 1.5 larger than the QMD and INDRA selection with $E_{trans} \geq 450 MeV$.

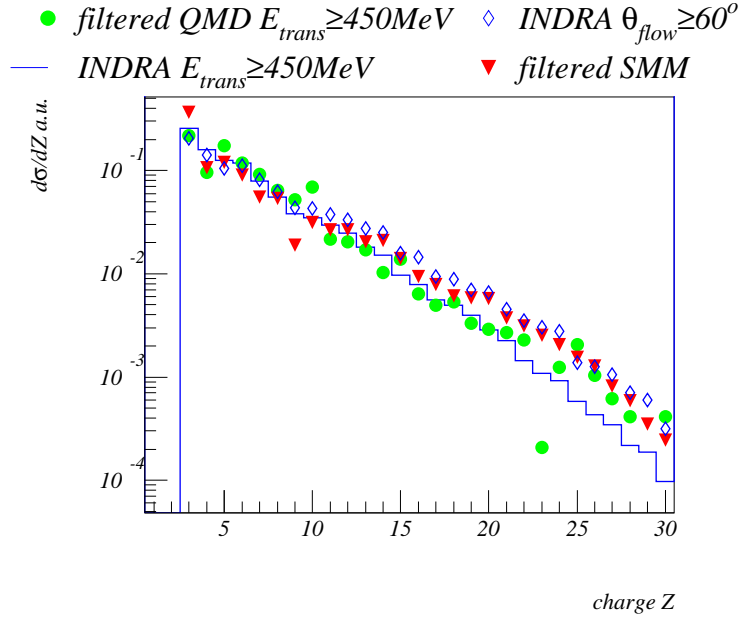


FIG. 10. Charge ($Z \geq 3$) distribution of INDRA for the events with $\theta_{flow} \geq 60^\circ$ and for events with $E_{trans} \geq 450 MeV$ as compared to QMD and SMM calculations.

Thus at midrapidity the charge distribution is well described by two almost opposite models for heavy ion collisions, the SMM, which starts out with the assumption that the system is in a global thermal equilibrium and the QMD which predicts, as we will see later, that the fragmentation is of dynamical origin. Hence the charge distribution at midrapidity is not sensitive to the reaction mechanism.

B. Azimuthal distribution in the event plane

Another variable for which statistical models make a very definite prediction is the azimuthal distribution of fragments. In order to determine the azimuthal distribution of QMD and INDRA events we have first to define an event plane with respect to which the azimuthal angle is measured. The event plane is defined by the beam axis and the largest eigenvector of the momentum tensor (equation (12)) for the filtered QMD and for the INDRA data. Using this definition of the event plane we observe the azimuthal distribution displayed in fig. 11.

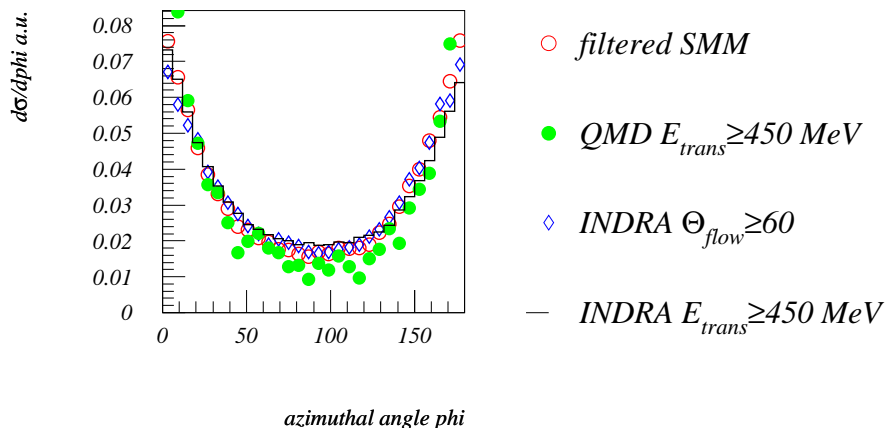


FIG. 11. Azimuthal distribution of fragments for the events with $\theta_{flow} \geq 60^\circ$ and for events with $E_{trans} \geq 450 \text{ MeV}$. We compare the INDRA results with QMD and SMM calculations

We see that in QMD and INDRA the fragments have a strong preference for being emitted in the event plane. Even if SMM does not have an event plane, we have to treat it in the same way as the QMD and INDRA data. Applying the routine to SMM, [1,22] we get surprisingly the same result: a preferred emission at the "reaction plane" and not as expected an isotropic emission. For low fragment multiplicities the diagonalisation of the momentum tensor produces always a preferred emission direction (an autocorrelation), even in case of a statistical emission. Hence the azimuthal distribution of fragments is another observable which does not allow to distinguish between thermal and dynamical emission of fragments.

C. Energy spectra and temperatures

In figure 12, top, we display the average transverse kinetic energy of fragments with respect to the beam direction emitted at midrapidity for the INDRA data and for QMD calculations. We observe a linear rise up to a charge of twelve, for bigger fragments where the Coulomb interaction between fragment and system becomes more important, the kinetic energy is independent of the fragment size. In the case of an emission from a pure thermal source one expects besides the modification due to the Coulomb repulsion [21] the average kinetic energy of the fragments to be independent of the fragment mass. The Coulomb repulsion is not sufficient to explain the increase of the energy with the fragment mass, therefore the experimental data contradict to a pure thermal emission scenario. However, assuming a radial flow proportional to the fragment mass this can be cured.

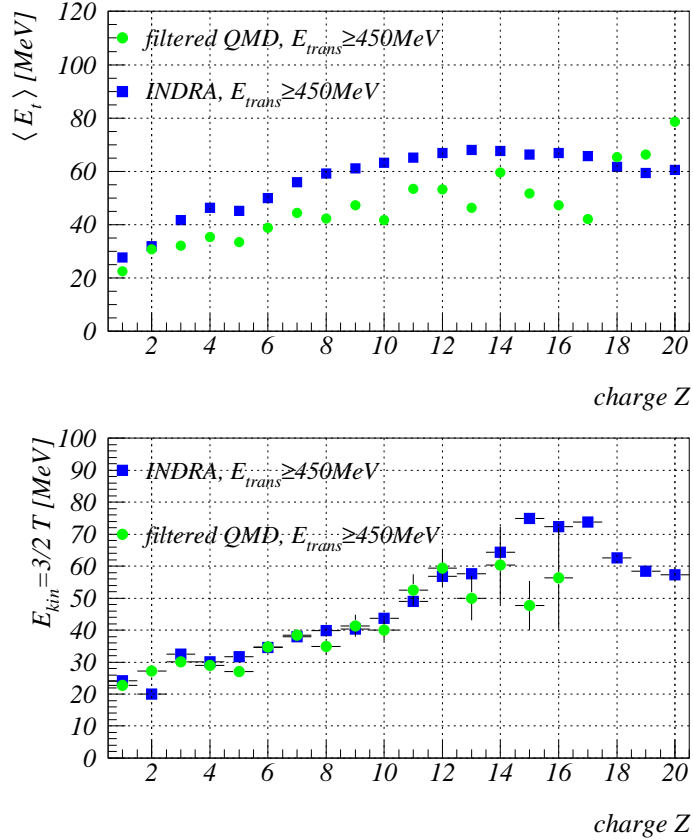


FIG. 12. *Top: Average transverse kinetic energy with respect to the beam axis as a function of the charge for fragments emitted in $60^\circ \leq \theta_{CM} \leq 120^\circ$. Bottom: Slope of the high energy tail of the energy distribution. We display INDRA data and QMD calculations. Error bars are suppressed.*

This linear increase of the kinetic energy is reproduced by the QMD data, the absolute value of the energy is, however, underestimated. The reason will be discussed later. In fig. 12, bottom, we display a fit to the exponential tail of the fragment kinetic energy spectra. For

thermal spectra this slope, being the temperature, has to be constant. We observe a slight increase of the slope as a function of the fragment charge and a good agreement between the INDRA data and the QMD simulations. For big fragments we have too little statistics to allow for a fit of the slope of the energy spectra obtained in QMD simulations. The slope of the INDRA data increases by almost a factor of 2 between $Z=10$ and $Z = 15$. For this increase there is no remedy in a thermal or a statistical model. Hence we encounter for the first time in the analysis of the midrapidity fragments an observable which manifests that the system is not in thermal equilibrium. Also the absolute value of the slope could hardly be associated with a temperature. The binding energy of nuclei is of the order of 8 MeV per nucleon. If the temperature is substantially higher than this value we do not expect that fragments survive. On the contrary, in the fast fragmentation model [14], we expect a slope of about $3/5 E_F$ which corresponds to the observed value for light fragments.

As the emission of fragments at midrapidity is a rare process which is logarithmically suppressed for large charges we do not have the statistics to compare in detail the kinetic energy spectra of fragments with a charge larger than 12. For higher charges the fluctuations render the analysis meaningless, for the slopes as well as for the spectra. The spectra for selected charges are presented in fig. 13. As already mentioned, the energy of the fragments in QMD simulations is too small as compared to the INDRA data. This points clearly to a caveat of the simulation program. As explained in section II the effective range of the nuclear interaction in QMD is too large as compared to reality. This has the consequence that the repulsive Coulomb force is compensated by the attractive Yukawa force up to large distances and hence the gain of kinetic energy due to the Coulomb potential is too small. This drawback of the QMD approach is also responsible for the low multiplicity at midrapidity. Many QMD fragments are not accepted because they are outside the detector acceptance. Because the effect of the Coulomb energy becomes more important with increasing charge, for larger charges the discrepancy between simulation and data becomes more important.

What is the origin of the increase of the average kinetic energy with the fragment mass, which is neither expected by a thermal model nor by an instantaneous fragmentation model? As we will see in these central collisions the system shows a quite important in-plane flow. This in-plane flow increases the transverse energy and depends on the fragment size. In a system which shows transverse flow the beam axis is not the proper axis of reference for measuring or calculating the transverse momentum but has to be replaced by the eigenvector of the momentum tensor

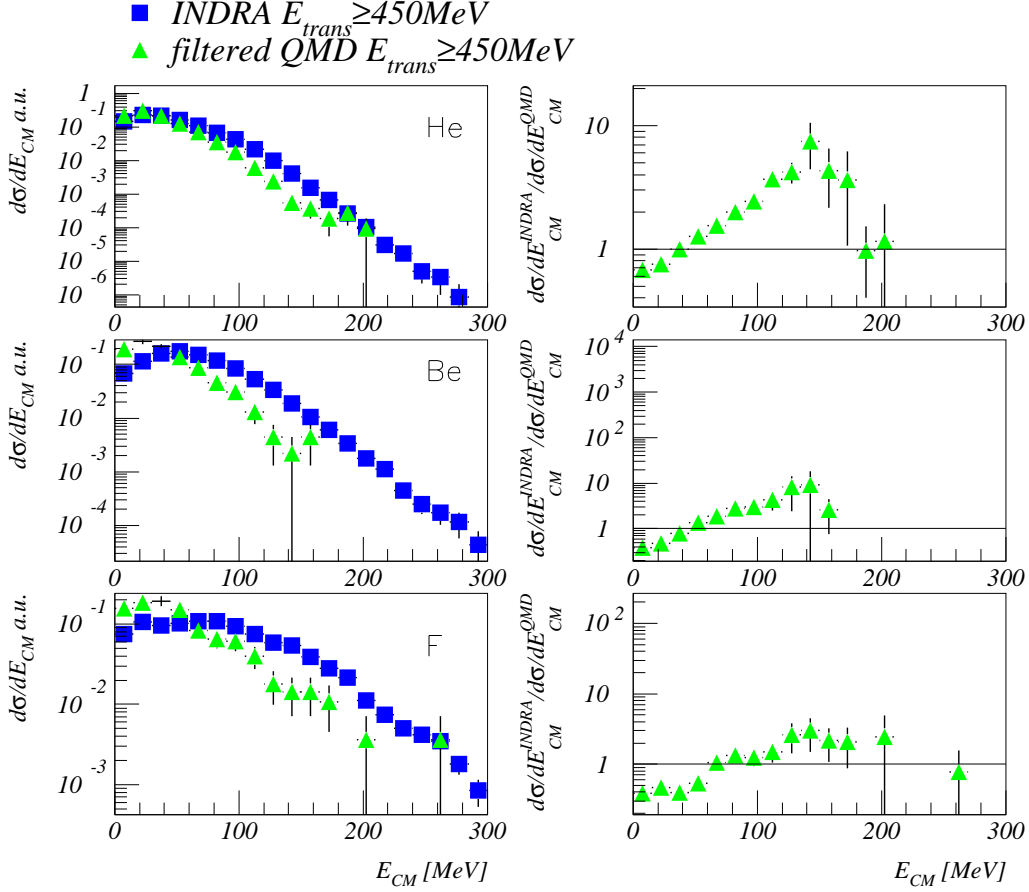


FIG. 13. Emission at $60^\circ \leq \theta_{CM} \leq 120^\circ$ Energy spectra: we compare the QMD and INDRA data. On the right hand side the spectra are displayed, on the left hand side the surprisal analysis.

$$P = \begin{pmatrix} \sum p_x^i p_x^i & \sum p_x^i p_y^i & \sum p_x^i p_z^i \\ \sum p_y^i p_x^i & \sum p_y^i p_y^i & \sum p_y^i p_z^i \\ \sum p_z^i p_x^i & \sum p_z^i p_y^i & \sum p_z^i p_z^i \end{pmatrix} \quad (12)$$

with the largest eigenvalue. Therefore we calculate this eigenvector for each INDRA and filtered QMD event for the detected IMF's and determined the transverse energy with respect to this eigenvector. The analysis is presented in fig. 14.

We see that in this rotated system the transverse energy becomes nearly independent of the fragment mass for charges larger than 3 and the absolute value for the largest fragments is almost half as large as compared to the value obtained with respect to the beam direction. Thus one has to conclude that the observed increase of the transverse energy with the fragment mass at midrapidity is nothing but a consequence of the in-plane flow and has nothing to do with a radial flow. Thus the conjecture to reconcile the data with statistical emission predictions by introducing a radial flow does not survive a detailed analysis. An in-plane flow as a non

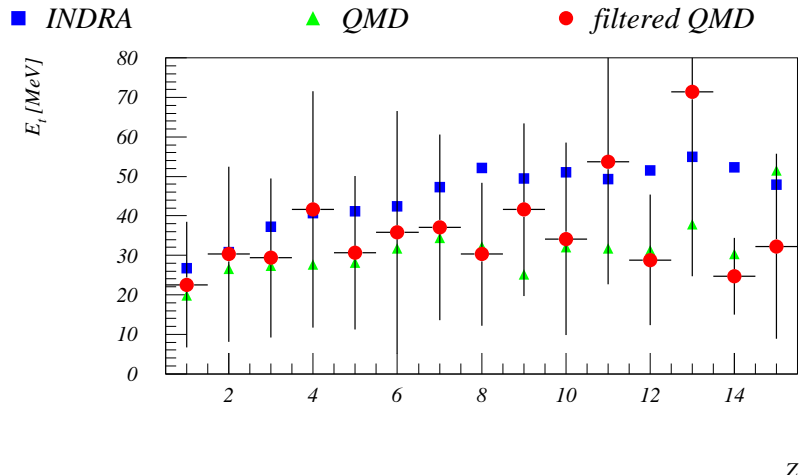


FIG. 14. *Transverse energy (with respect to the largest axis of the momentum tensor) of fragments observed in $60^\circ \leq \theta_{CM} \leq 120^\circ$. We compare filtered QMD simulations with experimental data, error bars are represented for filtered QMD only.*

equilibrium phenomenon is alien to a statistical model. The absolute value of the order 40 MeV would give a system "temperature" of 27 MeV, too large to be considered as the true temperature of the system.

In ref. [25] we could show that in QMD calculations the kinetic energy observed at midrapidity is a remnant of the initial Fermi-motion of the nucleons with an additional in-plane flow. The initial center of mass momentum of all nucleons which finally form a fragment is - up to the in-plan flow - almost exactly the same as that observed finally. The good agreement between our results and the data confirm these model predictions of the reaction mechanism.

In conclusion, in our analysis of the midrapidity energy spectra we found out that the mass dependence of the transverse energy is due to the in-plane flow of the fragments and not due to a radial flow as assumed in a statistical interpretation. The experimental spectra show a charge dependent slope which contradicts to the scenario of a thermal freeze out at a given density and temperature. The comparison with QMD suffers from the low number of fragments emitted at midrapidity. Due to an underestimation of the Coulomb barrier there are many fragments which are below the detector threshold.

IX. EMISSION OF FRAGMENTS AT FORWARD/BACKWARD

We come now to the emission at forward/backward direction. This region is characterized by a strong dependence of the fragment emission probability on the emission angle. It is therefore a region where the system has not even come close to thermal equilibrium and therefore it

presents the challenge whether simulation programs can predict this highly not equilibrated emission.

In forward/backward direction the kinetic energy as a function of the mass shows a steep linear rise in the QMD simulations as well as in the INDRA data, as displayed in fig. 15. For fragments with a charge lower than 10 INDRA and QMD agree quantitatively. For larger fragments, as discussed already, QMD overpredicts the kinetic energy because it generates large fragments with an unrealistic high in-plane flow. Due to this flow the fragments are passing the filter routine although in experiment these big fragments disappear in the beam pipe.

Comparing the average fragment kinetic energy in forward/backward direction (fig. 15) with that at midrapidity (fig. 12) we observe a much larger average energy and the average energy increase in forward/backward direction. This has to be viewed as a clear manifestation of the projectile and target character of these fragments.

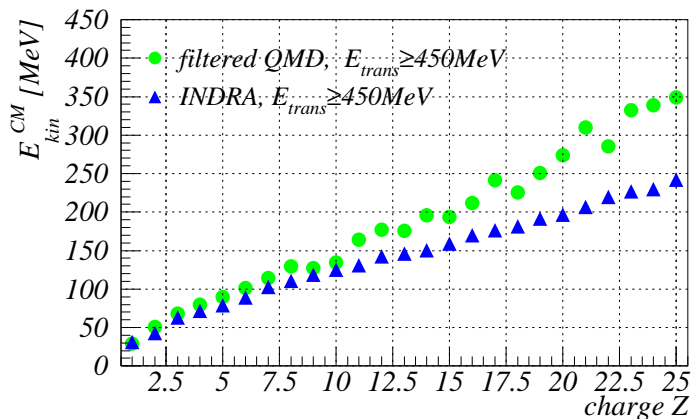


FIG. 15. *Central Collisions ($E_{trans} \geq 450$ MeV). Average kinetic energy for fragments emitted in forward/backward direction, the error bars are suppressed*

For a more detailed comparison of theory and data we analyze the kinetic energy spectra for fragments emitted in the forward/backward zone. We display the filtered QMD and INDRA kinetic energy spectra for different charges, $Z=5, 10$ and 18 in figure 16. On the left hand side we show the energy spectra, on the right hand side the result of the surprisal analysis. First we will focus on the INDRA spectra. With increasing mass (charge) the maximum of the spectra is shifted towards higher energies. The maximum of the distribution in forward/backward direction is located already at about 80% of the beam velocity (displayed as a line) and shows therefore clearly that most of the fragments are projectile/target like remnants despite of the fact that in these central collisions the fragments passed through the whole collision partner.

As can be seen from the spectra the increasing average kinetic energy is not only due to a shift of the maxima. The slopes change too: the larger the fragment the larger the slope. For

the case of the Ar fragments one observes already the overprediction of fragments close to the beam energy in QMD. The low energy part of the spectra is well reproduced, however.

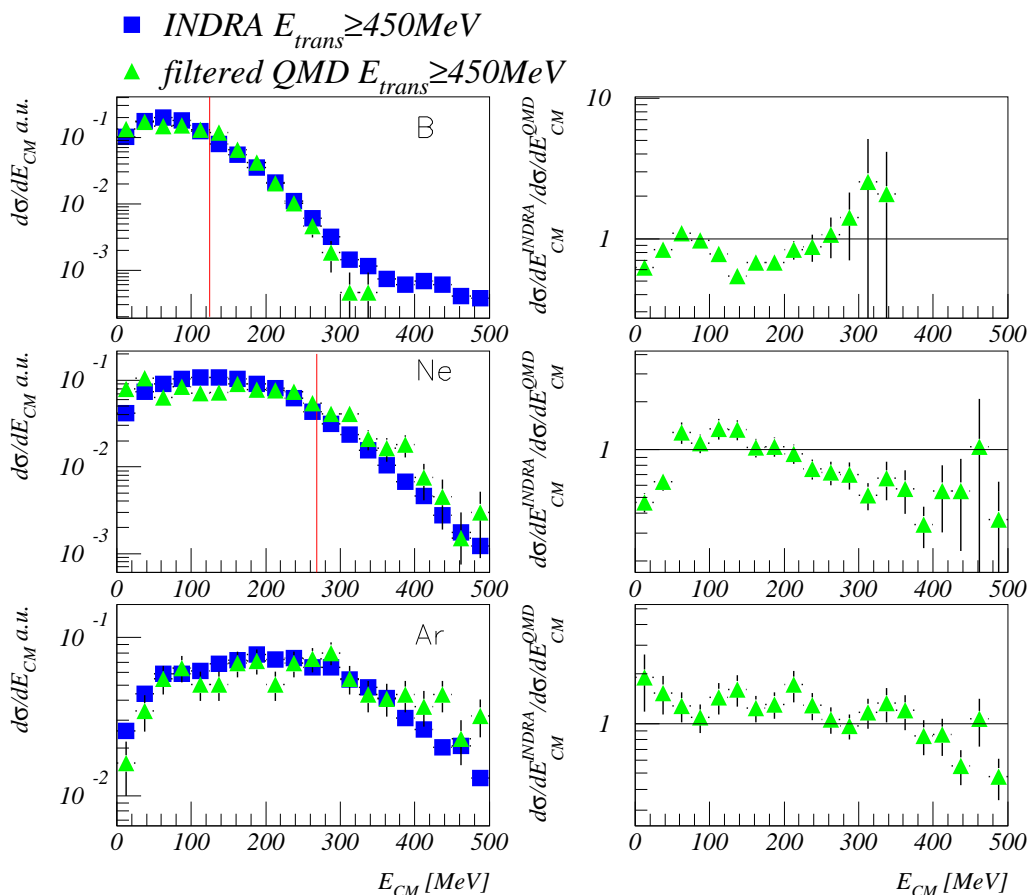


FIG. 16. *Central Collisions ($E_{trans} \geq 450$ MeV). Energy spectra for INDRA and QMD data in forward/backward direction in the center of mass frame. On the right hand side we display the logarithm of the ratio of the two spectra. The vertical lines corresponds to fragments having the beam velocity.*

X. OTHER EVENT SELECTION CRITERIA

As already stated there exist other criteria for finding central events. Here we follow the assumption of ref. [21,23] that all those events whose flow angle is larger than 60° can be considered as coming from a central collision. We find it useful to analyze several observables for this criterion.

We start our analysis with figure 17 in which we display the correlation between the total transverse energy of light particles as defined in section IV and the in-plane flow angle of the observed intermediate mass fragments which serves as criterion in the first conjecture. On the

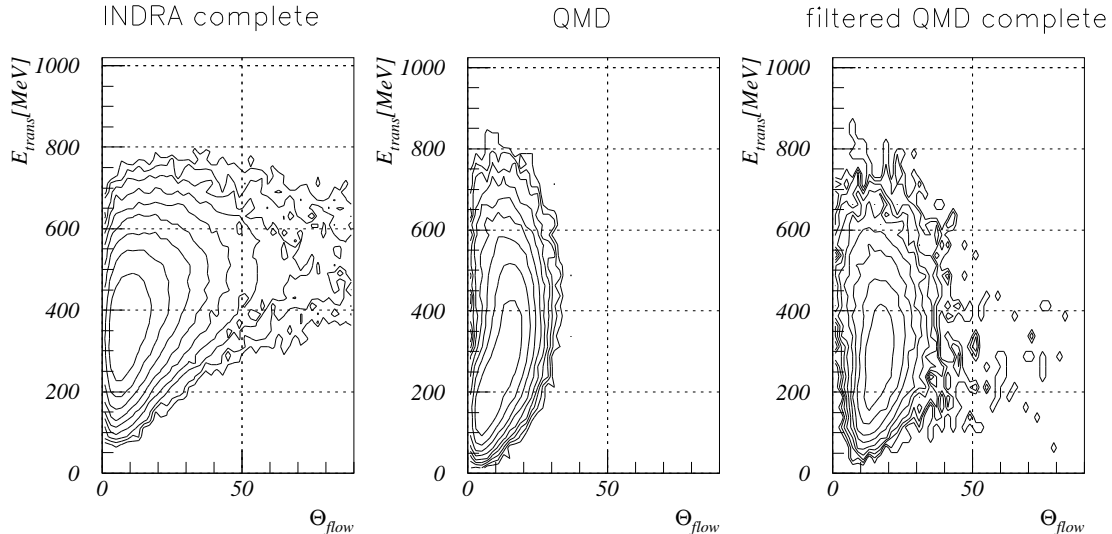


FIG. 17. Total transverse energy of light particles versus angle of flow of the fragments, we display complete INDRA (lhs) and QMD (rhs) data. The contour in z is logarithmic.

right hand side we see the filtered QMD results, in the middle the unfiltered QMD events and on the left hand side the result of the experiment [24]. The presentation is logarithmic in z . In order to be accepted 80% of the initial charge has to be detected in experiment as well as in filtered QMD events. We see once more the consequences of the too large in-plane flow angle of heavy fragments. The heavy fragments in the QMD simulation with the large in-plane flow which have already made problems in analyzing the central events spoil also the spectra obtained under the completeness criterion. Many of those almost binary events have a small flow and a small transverse energy E_{trans} , i.e. a large impact parameter. These events shift the maximum of the cross section to too low transverse energies.

We observe as well that there are too few QMD events with a large flow angle as compared to experiment. There about 2% of complete events show a flow angle larger than 60° whereas in QMD there are only 0.4%. The reason for this discrepancy is not easy to determine as one can see from the figure in the middle where the unfiltered complete QMD events are displayed. In the filtered simulation the large flow angle is due to the loss of some fragments, the completeness criterion ensures that these are only small fragments. In the unfiltered simulations the flow angle of these events is much smaller, shows only small fluctuations and never exceeds 60° .

There is only a weak correlation between the two centrality selection criteria as may be seen from fig. 18. There we display the transverse energy distribution of events with a flow angle larger than 60° . We see that this selection covers a large range of transverse energies extending well below $E_{trans} = 450\text{MeV}$ but misses on the other hand a large fraction of events with

$E_{trans} \geq 450 \text{ MeV}$. As can be inferred from fig. 4 both criteria cover a quite different range of impact parameters and therefore we should not expect that both criteria give the same results.

The criterion that the flow angle has to be larger than 60° covers - according to QMD - a wider impact parameter range.

In view of these facts it is remarkable that most of the observables are very similar for both criteria. This is even true for the kinetic energy spectra for fragments emitted at midrapidity.

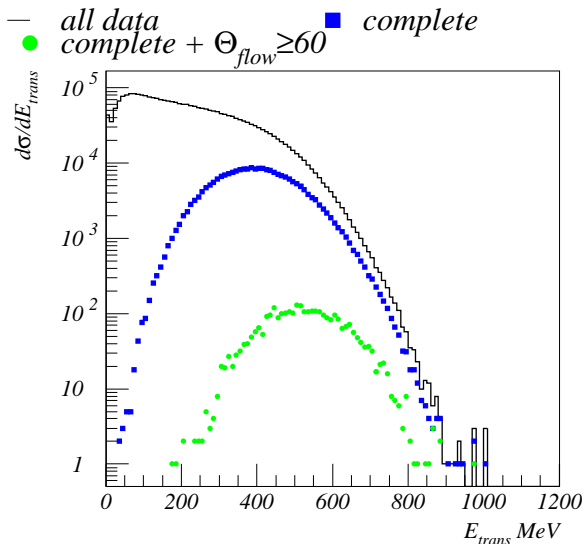


FIG. 18. *INDRA*: distribution of E_{trans} for all data, complete events and events with $\theta_{flow} \geq 60^\circ$

XI. REACTION SCENARIO AND CONCLUSIONS

The recently measured reaction $\text{Xe}(50\text{A MeV})+\text{Sn}$ is at the moment the most complete experiment on multifragmentation. We have presented a very detailed comparison between the QMD calculations and the experimental results. We found for most of the observables a quantitative agreement between the simulations and the experiment. The QMD simulations has one essential shortcoming which become relevant in quantitative comparisons on the level which is possible with these new data. It underpredicts the repulsive Coulomb repulsion and overpredicts the attractive nuclear interaction due to a range of the nuclear force which is too large as compared to reality. As an immediate consequence we observe too small kinetic energies and larger in-plane flow of the fragments as compared to the experiment. The too large in-plane flow influences , despite of its small value, a whole chain of observables. Heavy fragments which in reality disappear in the beam pipe are now observed due to their large in-plane flow. Therefore the mass yield of QMD disagrees with experiment for charges larger than 30. The events with large remnants have usually a small charged particle multiplicity.

Hence the artificial acceptance of those events lowers the multiplicity of LCP's, however it does not change the form of IMF observables because IMF's are not produced in these events.

QMD simulations reveal as the experiment that even central collisions show a binary character. Thus the stopping power of nuclear matter at this energy is smaller than at lower energies as well as at higher energies. At this energy we observe the transition between mean field dominated stopping (as observed at lower energies yielding compound nucleus formation) and collision dominated stopping (as observed at higher energies where a fireball is formed). In this transition region the beam energy is too large for a stopping by the mean field and too small for a stopping by collisions because most of the collisions are still Pauli suppressed.

Although in the midrapidity zone the angular distribution is flat and the energy per particle constant, the matter there is far from equilibrium. A detailed analysis reveals a strong in-plane flow and a strong azimuthal anisotropy. With respect to the largest eigenvector of the momentum tensor the average transverse kinetic energy of the fragments is constant [25]. The linear increase as a function of the fragment mass observed with respect to beam axis (fig. 12), which has been interpreted as a sign of a collective radial flow, is merely a consequence of the in-plane flow of fragments.

For several observables we have seen discrepancies to the INDRA data. These discrepancies are related to shortcomings of the QMD simulation which could be identified. Besides this we observe a quite good agreement between data and theory and it becomes useful to take advantage of the additional coordinate space and time information available in the QMD simulations. A detailed analysis of the time evolution has been published elsewhere [25]. It reveals that the final momentum - besides the in-plane flow - of the fragments is almost exactly that of its progenitor at the beginning of the reaction. Along the eigenvector of the flow tensor the initial average momentum of those nucleons which form finally a fragment does change but arrives finally at its initial values. Hence all changes during the reaction are collective which affects all fragment nucleons in the same way and is caused by the potential interactions. There is no room for a random (thermal) excitation. Thus the process is in momentum space very close to that proposed by Goldhaber 25 years ago: the fragment transverse kinetic energy is a consequence of the initial Fermi energy. It is a convolution of the momenta of the entrained nucleons, each of them having the momentum distribution of nucleon in a Fermi gas.

Goldhaber assumed that the fragmentation is a fast process. This we cannot confirm. The fragments decouple from the system only after 200 fm/c. Therefore the question remains how the fragments pass the surrounding matter without being destroyed. The two body potential interaction is rather smooth and acts on all fragment nucleons very similar. Hard two body

collisions may transfer momentum to one of the fragment nucleons what may lead to a separation of that nucleons from the other fragment nucleons. The key quantity to understand this passing trough is the mean free path. At the energies considered here it is quite large due to the Pauli suppression of the collision. Therefore in a very simplified model, which contains however the essential physics, multifragmentation can be viewed as two lattices, representing the nuclei, passing through each other. Each lattice site is occupied by a nucleon. Collisions transfer momentum, the scattered nucleons escape and leave holes at the corresponding lattice sites. If sufficient but not too many holes are created the lattices separate into disconnected parts, which are the fragments. If more collisions occur there are more holes and consequently less fragments, if less collisions occur we have only connected parts,i.e. remnants of projectile and target. Thus nucleons being finally part of fragments have only suffered from small momentum transfers during the collision, or, inversely, nucleons which had had a hard collisions are not part of a fragments. Of course in reality the situation is much more complicated because the nucleons have momenta but these additional features do not change the qualitative description.

This scenario is also the basis of the success of the percolation model which describes multiplicity distributions and the charge yield of multifragmentation quite satisfying. The detailed investigation of how the fragments pass the surrounding matter has been performed in ref. [26] long before data became available. That this reaction scenario is now confirmed by experiment demonstrates that the simulations of heavy ion reactions at this energy has reached a level which allows to draw firm conclusions about the underlying reacting mechanism and allows to understand the evolution of the finite number non equilibrium quantum systems.

It is remarkable that statistical models yield - in the limited kinematical regimes where they can be applied - almost the same value for the different observables. This has been interpreted in the past as a strong indication that the system comes to a global equilibrium. This we cannot confirm. In view of our results this agreement is inconclusive as far as the reaction mechanism is concerned.

-
- [1] J.P. Bondorf, A.S. Botvina, A.S. Iljinov, I.N. Mishustin, K. Sneppen, Phys. Rep. **257** 133 (1995)
 - [2] D.H.E Gross, Rep. Prog. Phys. **53**, 605 (1990), and references therein.
 - [3] L.G. Moretto and G.J. Wozniak, Annual Reviews of Nuclear and Particle Science, J.D. Jackson, ed., **43**, 379 (1993).

- [4] R. Bougault, Proceedings of the International Winter Meeting in Nuclear Physics, Bormio (Italy) 1997
- [5] M. F. Rivet et al., Phys. Lett. **B 430**, 217 (1998)
- [6] D. Hahn and H. Stöcker, Nucl. Phys. **A 476**, 718 (1988)
- [7] J. Aichelin, J. Hüfner and R. Ibarra, Phys. Rev. **C 30**, 107 (1984).
- [8] M. Petrovici et al., Phys. Rev. Lett. **74**, 5001 (1995).
- [9] S.C. Jeong et al., Phys. Rev. Lett. **72**, 3468 (1994)
- [10] B. Tsang, Proceedings of the International Workshop XXII on Gross Properties of Nuclei and Nuclear Excitations, Hirschegg, Austria, January 17 -22, 1994 ed by H. Feldmeier and W. Nörenberg
- [11] C. Ogilvie, Phys. Rev. Lett **67** (1991) 1214
- [12] Schüttauf et al. Nucl. Phys. **A 607** (1996) 457
- [13] W. Reisdorf et al. Nucl. Phys. **A 612** (1997) 493
- [14] A.S. Goldhaber, Phys. Lett. **53B** (1974) 306
- [15] G. Peilert et al. Phys. Rev. **C 39** (1989) 1402
- [16] J. Aichelin, Phys. Rep. **202**, 233 (1991), and references therein.
- [17] C. Hartnack et al. Eur. Phys. J. **A 1** (1998) 151
- [18] J.Lukasik Phys. Rev. **C 55** (1997) 1907
- [19] O. Tirel, G. Auger (GANIL Caen), private communication
- [20] N. Marie et al. Phys. Lett. **B 391** (1997) 15
- [21] S. Salou, Thesis, U Caen, GANIL T 97 06
- [22] A.S. Botvina et al., Nucl. Phys. **A 584**, 737 (1995)
- [23] A. Le Fevre, Thesis, U Paris 7, GANIL T 97 03
- [24] A. Nguyen et al., Proceedings of the International Winter Meeting in Nuclear Physics, Bormio (Italy) 1998
- [25] R. Nebauer and J. Aichelin, submitted to Nucl. Phys. A., nucl-th/9807064

[26] P.-B. Gossiaux et. al., Nucl. Phys. **A619** 379 (1997)